Gold Nanoclusters

DOI: 10.1002/anie.201302926

Superatom Networks in Thiolate-Protected Gold Nanoparticles**

Longjiu Cheng, Yuan Yuan, Xiuzhen Zhang, and Jinlong Yang**

Owing to their unique properties, thiolate-protected gold nanoparticles (Au-SR) with core diameters of less than 2 nm are of importance and have attracted interest both experimentally and theoretically.[1]

Geometric shell closure is an important factor for the stability of Au-SR nanoparticles, and the geometries are unique as a result of the strong relativistic effects of Au element. The seminal X-ray crystal structural determination of $[Au_{102}(SR)_{44}]$ showed that the thiolate ligands do not simply passivate a large gold core but instead form $[Au(SR)_2]$ and $[Au_2(SR)_3]$ oligomers that bind to a smaller gold core,[2] in agreement with the previous "divide-and-protect" model.[3] Later, in the crystal structures of $[Au_{25}(SR)_{18}]^-$, $[Au_{38}(SR)_{24}]$, and $[Au_{36}(SR)_{24}]$ compounds,[4–6] the model of a gold core surrounded by $[Au_n(SR)_{n+1}]$ oligomers was further confirmed.

Besides the four crystallized Au-SR compounds, there are also a variety of Au-SR compounds which are experimentally isolated and measured by mass and/or optical spectra but not crystallized yet, such as $[Au_{44}(SR)_{28}]^{2-}$,[7] $[Au_{144}(SR)_{60}]$,[8] $[Au_{12}(SR)_9]^+$,[9] $[Au_{18}(SR)_{14}]$,[10] $[Au_{20}(SR)_{16}]$,[11] $[Au_{24}(SR)_{20}]$,[12] $[Au_{40}(SR)_{24}]$,[13] $[Au_{19}(SR)_{13}]$,[14] and $[Au_{68}(SR)_{34}]$.[15] Structures of the experimentally isolated Au-SR compounds can be theoretically predicted by density functional theory (DFT) calculations. Based on the "divide-and-protect" model, knowledge of the bonding motifs of $[Au_{25}(SR)_{18}]^-$ and $[Au_{38}(SR)_{24}]$ was given by DFT predictions[16] independent of and in agreement with X-ray crystal-structure determination. DFT predictions have successfully located the structures for many of the synthesized compounds in agreement with the experimental X-ray diffraction and/or UV/Vis spectra, for example, $[Au_{40}(SR)_{24}]^{2-}$,[17] $[Au_{144}(SR)_{60}]$,[18] $[Au_{12}(SR)_9]^+$,[19] $[Au_{18}(SR)_{14}]$,[20] $[Au_{20}(SR)_{16}]$,[21] $[Au_{24}(SR)_{20}]$,[22] and $[Au_{19}(SR)_{13}]$.[23] All of these Au-SR clusters show geometric shell closure following the "divide-and-protect" model and have molecule-like electronic structures with a relatively large gap between the highest occupied–lowest unoccupied molecular orbitals (HOMO–LUMO).

In addition to the geometric shells, electronic shell closure is another important factor for the stability of Au-SR nanoparticles. To understand the intrinsic stability of Au-SR clusters, the superatom model was suggested by Hakkinen and co-workers.[24] The jellium model for metal clusters with electronic shell closure was first proposed to explain the high abundance of certain magic-number alkali-metal clusters observed in the mass experiments.[25] In this model, the valence electrons of a cluster are delocalized in the cluster volume and fill discrete energy levels. Based on such a jellium model, exceptional stability of Au-SR clusters is associated with the magic numbers of free valence electrons ($n^* = 2$, 8, 18, 34, 58, 92,...).[24] The total number of free valence electrons associated with a Au-SR cluster $Au_M(SR)_N{}^q$ can be counted based on the formula $n^* = M-N-q$, where M is the number of Au($6s^1$) electrons, N and q are the number of electron-withdrawing ligands (thiol groups) and the charge state of the cluster, respectively. Based on the superatom model, stability of the experimentally measured clusters can be understood with the magic numbers, such as $[Au_{102}(SR)_{44}]$ (58e),[2] $[Au_{68}(SR)_{34}]$ (34e),[15] $[Au_{44}(SR)_{28}]^{2-}$ (18e),[7] $[Au_{25}(SR)_{18}]^-$ (8e),[4] and $[Au_{12}(SR)_9]^+$ (2e).[9] These clusters both have a spherical and symmetric gold core.

However, not all experimentally produced Au-SR clusters exhibit magic numbers of free valence electrons as described by the spherical jellium model. $[Au_{38}(SR)_{24}]$ is a highly stable cluster that has been detected in many experiments under different reaction conditions, but the 14 free valence electrons disagree with the magic numbers of superatom model. Electronic stability of the 14e prolate Au_{23} core of $[Au_{38}(SR)_{24}]$ was first explained using Clemenger's ellipsoidal shell model[26] by Zeng and co-workers,[16b] where 14e is a magic number in the ellipsoidal shell model. Lately, the electronic stability of $[Au_{38}(SR)_{24}]$ was further explained by Aikens et al.[16c] using the particle-in-a-cylinder model, a variation of the ellipsoidal shell model. However, the ellipsoidal model is based on an oblate shape, which is structureless and different from the prolate shape of $[Au_{38}(SR)_{24}]$. Very recently, Cheng and Yang[27] proposed a super valence bond (SVB) model to explain the electronic stability of non-spherical shells of metal clusters, and found that Li_8, Li_{10}, and Li_{14} are exact analogous of CH_4, N_2, and F_2, respectively, in electronic state and bonding patterns. Using the SVB model, the 23-center 14-electron (23c-14e) bi-icosahedral Au core of $[Au_{38}(SR)_{24}]$ is shown to be a superatomic molecule (super F_2) in electronic shells.[28]

[*] Prof. L. Cheng, Y. Yuan, X. Zhang
Department of Chemistry, Anhui University
Hefei, Anhui, 230039 (P. R. China)
E-mail: clj@ustc.edu
Prof. J. Yang
Hefei National Laboratory for Physics Sciences at the Microscale
University of Science & Technology of China
Hefei, Anhui, 230026 (P. R. China)
E-mail: jlyang@ustc.edu.cn

[**] We thank Professor Boldyrev for the AdNDP codes. This work is financed by the NSFC (21121003, 21273008, 21233007, 91021004), by the National Key Basic Research Program of China (2011CB921404), by the Chinese Academy of Sciences (XDB01020300),and by the outstanding youth foundation of Anhui University. The calculations are carried out on the High-Performance Computing Centre of Anhui University.

Supporting information for this article (full citation of Ref. [34], AdNDP chemical bonding of $[Au_{18}(SH)_{14}]$ and $[Au_{24}(SH)_{20}]$, detailed aromaticity analysis for $[Au_{20}(SH)_{16}]$, and coordinates of **t1–t4**) is available on the WWW under http://dx.doi.org/10.1002/anie.201302926.

Exceptions were also found for some other clusters such as $[Au_{18}(SR)_{14}]$, $[Au_{20}(SR)_{16}]$, and $[Au_{24}(SR)_{20}]$.[10–12] The three compounds have both four free valence electrons in the gold core, which disagrees with the counts of magic numbers in the superatom model, but are electronically very stable with large HOMO–LUMO gaps in about 1.6 eV, 2.1 eV, and 1.5 eV, respectively.[10–12] The three 4e compounds have been isolated and measured by mass and optical spectra but their geometric structures are still not determined by X-ray measurement. A probably geometric structure of $[Au_{20}(SR)_{16}]$ has been predicted by Pei et al.[21] using DFT calculations in good agreement with the experiment in optical spectra and HOMO–LUMO gap. The predicted structure can be viewed as a prolate Au_8 core "stapled "by four $[Au_3(SR)_4]$ oligomers, of which the Au_8 core can be viewed as the fusion of two tetrahedral Au_4 units through edges. Very recently, structures of the $[Au_{18}(SR)_{14}]$ cluster[20] and $[Au_{24}(SR)_{20}]$ cluster[22] were also theoretically predicted in good agreement with the experimental optical spectra and HOMO–LUMO gaps, and the prolate Au_8 core was further confirmed in the two compounds.

To explain the electronic stability of these 4e compounds, Clemenger's ellipsoidal shell model was also suggested based on the prolate shape.[21] However, 4e seems not to be a magic number in the ellipsoidal shell model. Also, the electronic stability of the 4e compounds cannot be understood by the SVB model. Thus, there must be another story to be uncovered for the electronic shell closure of these 4e compounds.

Herein, we propose the concept of superatom-network (SAN) to understand the "magic" stability of these 4e compounds. Based on the SAN model, as shown in Figure 1, these 4e compounds should be taken as a network of two 4c–2e tetrahedral Au_4 superatoms stapled by four $[Au_n(SR)_{n+1}]$ ($n = 3, 4, 5$) oligomers, where Au–Au interactions between superatoms are mainly non-bond interactions.

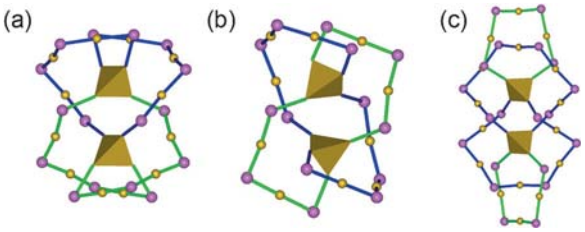

Figure 1. Superatom-network model for a) $[Au_{20}(SR)_{16}]$, b) $[Au_{18}(SR)_{14}]$, and c) $[Au_{24}(SR)_{20}]$. R groups are removed for clarity. The staple motifs are given as ball-and-stick models (Au yellow, SR pink), the sticks are shown in different colors for clarity. The 4c–2e tetrahedral Au_4 superatom cores are shown as polyhedral models. Coordinates are from Ref. [20, 22]].

We first focus on the atomic structure of the Au_8^{4+} core of the three 4e compounds. The Au_8^{4+} core of $[Au_{20}(SR)_{16}]$ has a D_2 symmetry. As shown in Figure 2, Au–Au bond lengths within the Au_4 tetrahedral unit are 2.76–2.84 Å, and the Au–Au distances between the two Au_4 tetrahedral units are clearly longer at 3.06 Å and 3.12 Å. The Au_8^{4+} core of $[Au_{18}(SR)_{14}]$ is in C_1 symmetry, where bond lengths within the two Au_4 tetrahedrons are 2.76–2.88 Å and 2.75–2.83 Å, and the Au–Au distances between two tetrahedral units are also longer at 2.95–3.15 Å. Atomic structure of the Au_8^{4+} core of $[Au_{24}(SR)_{20}]$ is very similar to that of $[Au_{20}(SR)_{16}]$, where Au–Au lengths within and between the Au_4 tetrahedral units are 2.76–2.82 Å and 3.11–3.16 Å respectively (all in Figure 2). The interactions between nearest-neighbor non-bond Au atoms are much stronger than to other metals and the non-bond distances are also much shorter (they can be only slightly longer than the Au–Au bonded lengths) as a result of the strong relativistic effects. Thus, we suspect that such a Au_8^{4+} core should be viewed as two non-conjugate 4c–2e tetrahedral Au_4 superatoms based on the geometry.

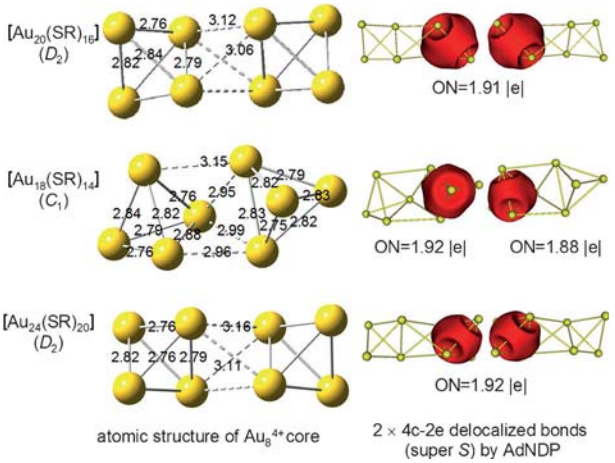

Figure 2. a) Atomic structures (left) and AdNDP localized chemical bonding (right) of the Au_8^{4+} core of $[Au_{20}(SR)_{16}]$ (top), $[Au_{18}(SR)_{14}]$ (middle), and $[Au_{24}(SR)_{20}]$ (bottom). The distances (Å) between and within Au_4 tetrahedrons are given. The Au(5d) lone-pairs (LPs) are not shown.

To verify the SAN model in the Au_8^{4+} core we selected the adaptive natural density partitioning (AdNDP) method as a tool for chemical bonding analysis. This method was developed by Zubarev and Boldyrev[29] and used to analyze chemical bonding in organic molecules, boron clusters, and Au clusters.[30] AdNDP recovers both Lewis bonding elements (1c–2e and 2c–2e objects) and delocalized bonding elements (*n*c–2e), an approach which achieves seamless description of systems featuring both localized and delocalized bonding. As shown in Figure 2, in each case of the three 4e compounds, chemical bonding analysis given by AdNDP reveals two non-conjugate 4c–2e delocalized bonds in each Au_4 tetrahedral unit. They only differ little at the occupancy numbers (ON = 1.88–1.92 | e |). The Au(5d) lone-pairs (LPs) with ON = 1.93–2.00 | e | are not shown. AdNDP analysis confirms that the prolate Au_8^{4+} core consists of two separated Au_4^{2+} close-shell 2e superatoms.

Ligand effects are also very important for Au-SR clusters. Next, we give a total bonding analysis of $[Au_{20}(SR)_{16}]$ using AdNDP. The R groups do not affect much of the overall bonding patterns of the compound, thus we use SH instead of SR for simplicity and clarity in chemical bonding analysis.

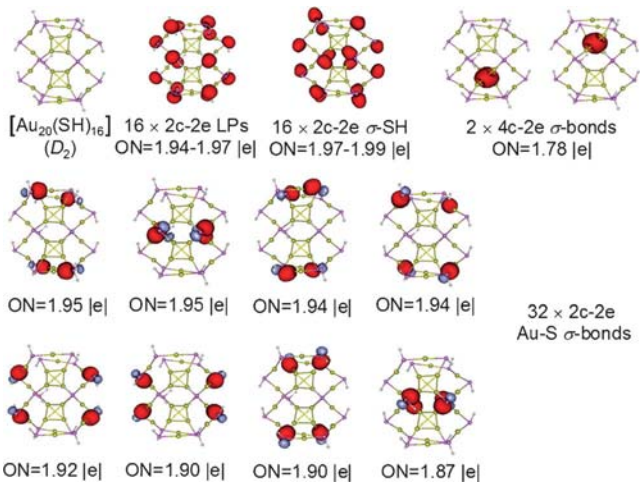

Figure 3. Geometry (Au yellow, S pink, H white) and AdNDP localized natural bonding orbitals (red-gray) of the valence shells of $[Au_{20}(SH)_{16}]$.

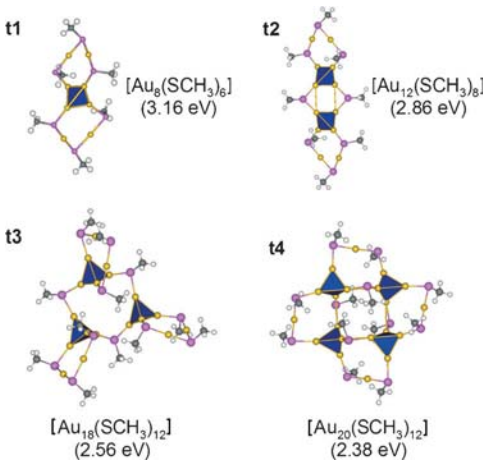

Figure 4. Modeled Au-SCH_3 clusters in 1×2e (**t1**, $[Au_8(SCH_3)_6]$), 2×2e (**t2**, $[Au_{12}(SCH_3)_8]$), 3×2e (**t3**, $[Au_{18}(SCH_3)_{12}]$), and 4×2e (**t4**, $[Au_{20}(SCH_3)_{12}]$) SAN networks (Au yellow, S pink, C gray, H white). The tetrahedral 2e superatoms are highlighted in dark blue. HOMO–LUMO energy gaps are in parentheses.

Figure 3 plots the bonding framework of the valence shells of $[Au_{20}(SH)_{16}]$ of AdNDP analysis. As expected, the Au(5d) orbitals are viewed as LPs with ON = 1.88–1.99 | e | , which are excluded in this analysis. AdNDP analysis reveals sixteen LPs of S atoms (ON = 1.94–1.97 | e |), sixteen 2c–2e localized SH σ-bonds (ON = 1.97–1.99 | e |), and thirty-two 2c–2e localized AuS σ bonds (ON = 1.87–1.95 | e |). The remaining four electrons are delocalized in each tetrahedral Au_4 unit as 4c–2e σ bonds with ON = 1.78 | e | . The total bonding analysis of $[Au_{20}(SH)_{16}]$ confirms the SAN model in electronic shells. The chemical bonding in $[Au_{18}(SH)_{14}]$ and $[Au_{24}(SH)_{20}]$ are very similar to that of $[Au_{20}(SH)_{16}]$, of which SAN model is viewed by AdNDP analysis in a straightforward manner (Supporting Information, Figure S1).

Aromaticity is now a popular measurement for shell-closure of delocalized bonding by calculating the nucleus-independent chemical shifts (NICS) values.[31] The NICSzz-scan curve of $[Au_{20}(SH)_{16}]$ along the D_2 axis shows clearly that the Au_8 core consists of two independent superatoms, which gives extra support to the SAN model (Supporting Information, Figure S2).

In addition to the three 2×2e compounds discussed herein, there must be other Au-SR compounds with electronic structures corresponding to the SAN model. To confirm this suspicion, we modeled some $n\times2$e Au-SR clusters (n = 1–4, R = CH_3) following the SAN model. As shown in Figure 4, the 1×2e compound (**t1**, $[Au_8(SCH_3)_6]$) consists of one tetrahedral 2e superatom and two $\{Au_2(SCH_3)_3\}$ staple motifs with a very large HOMO–LUMO gap of 3.16 eV; the 2×2e compound (**t2**, $[Au_{12}(SCH_3)_8]$) consists of two 2e superatoms linked by two $\{Au_2(SCH_3)_3\}$ and two SCH_3 staple motifs with an energy gap of 2.86 eV; the 3×2e compound (**t3**, $[Au_{18}(SCH_3)_{12}]$ consists of three 2e superatoms linked by three $\{Au_2(SCH_3)_3\}$ and three SCH_3 staple motifs with an energy gap of 2.56 eV; the 4×2e compound (**t4**, $[Au_{20}(SCH_3)_{12}]$) consists of four 2e superatoms linked by four $\{Au(SCH_3)_2\}$ and four SCH_3 staple motifs with an energy gap of 2.38 eV. These four $n\times2$e Au-SCH_3 clusters (**t1–t4**) are modeled as simply as possible, which may not be the global minimum structure, but have very stable electronic structures with large energy gaps and are true local minimum structures as verified by a frequency check.

The SAN model may be useful in finding some other experimentally produced Au-SR clusters, which are also exceptions for previous electronic-shell model, such as $[Au_{19}(SR)_{13}]$ (3×2e networks) and $[Au_{40}(SR)_{24}]$ (2×8e networks).[13,14] A structure for $[Au_{19}(SR)_{13}]$ has recently been predicted by Jiang[23] using a "staple fitness" method. However, only compact gold cores are assumed for the fitness and the HOMO–LUMO energy gap in the predicted structure is about 0.2 eV lower than the experimental value (ca. 1.5 eV). For Au-SR clusters, theoretically calculated gaps are usually slightly larger than the experimental values at the PBE/LANL2DZ level of theory. Thus we think that the real structure of $[Au_{19}(SR)_{13}]$ might also follow the SAN model, and the 3×2e core should be considered in "staple fitness".

Recently, a probable geometric structure of $[Au_{40}(SR)_{24}]$ has been determined by DFT prediction. Malola et al.[32] suggested that $[Au_{40}(SR)_{24}]$ is a combination of a Au_{26} bi-icosahedral cluster core with $6[Au(SR)_2]$ and $4[Au_2(SR)_3]$ oligomers, where the 16e bi-icosahedral Au_{26} core is explained by a 2×8e "superatom dimer". The concept of the "superatom dimer" is essentially telling the same story with our SAN model. However, the two parts of the bi-icosahedral core in $[Au_{40}(SR)_{24}]$ are clearly in closer proximity (2.82 Å) than the tetrahedra in our examples, and the interaction between the two icosahedral parts still needs to be further verified. In addition, the newly crystallized phosphine/thiolate-protected Au_{24} nanocluster[33] consists of two Au_{12} incomplete icosahedrons with two pentagonal planes joined together by five thiolate linkages, which may also be a 2×8e compound.

In summary, we proposed a SAN model to explain the electronic stability of the 4e compounds $[Au_{18}(SR)_{14}]$, $[Au_{20}(SR)_{16}]$, and $[Au_{24}(SR)_{20}]$. As the products of self-

assembly, the experimentally produced Au-SR clusters must be shell-closed species in terms of both their geometric and electronic structures. Unlike previous superatom and super valence bond models, the magic stability and large HOMO–LUMO gaps of these 4e compounds are explained by the SAN model. This model was supported by the analysis from Au–Au bond/non-bond lengths, AdNDP localized chemical bonds, and NICS-scan curves. The SAN model gives new physical insight into the chemical bonding of these 4e Au-SR compounds, which are viewed as "a network of two 2e-superatom gold cores" linked and stapled by four $\{Au_n(SR)_{n+1}\}$ staple motifs. The SAN model may be useful in understanding the stability of some other experimentally produced Au-SR clusters, which are also exceptions to previous electronic-shell models, such as $[Au_{19}(SR)_{13}]$ ($3\times2e$ networks). Moreover, based on the SAN model, the assembly of materials based on Au-cluster-superatoms and sulfur can be expected as extensions of SAN complexes.

Experimental Section

Computational details: Geometries of $[Au_{18}(SH)_{14}]$, $[Au_{20}(SH)_{16}]$, and $[Au_{24}(SH)_{20}]$ are relaxed by density functional theory (DFT) calculations performed on the Gaussian 09 package[34] starting from the lowest-energy isomers of $[Au_{18}(SCH_3)_{14}]$, $[Au_{20}(SCH_3)_{16}]$, and $[Au_{24}(SCH_3)_{20}]$, respectively, in Ref. [20,22]]. DFT geometry relaxations are performed using the generalized gradient approximation method developed by Perdew, Burke, and Ernzerhof (PBE)[35] with the LANL2DZ basis set for Au element and 6-31G* for other elements (PBE/LANL2DZ/6-31G*). Natural bonding analysis by AdNDP and aromaticity analysis by NICS are also performed at the same PBE/LANL2DZ/6-31G* level of theory. Molecular orbital (MO) visualization is performed using MOLEKEL 5.4.[36] **t1–t4** Au-SCH_3 isomers are relaxed at PBE/LANL2DZ/6-31G(d,p) level of theory, and the HOMO–LUMO energy gaps are also given in this level.

Received: April 9, 2013
Revised: May 23, 2013
Published online: July 14, 2013

Keywords: electronic stability · gold · nanoclusters · superatom network · super valence bond model

[1] a) R. Jin, *Nanoscale* **2010**, *2*, 343–362; b) M. M. Alvarez, J. T. Khoury, T. G. Schaaff, M. N. Shafigullin, I. Vezmar, R. L. Whetten, *J. Phys. Chem. B* **1997**, *101*, 3706–3712; c) Y. Negishi, K. Nobusada, T. Tsukuda, *J. Am. Chem. Soc.* **2005**, *127*, 5261–5270; d) S. Chen, R. S. Ingram, M. J. Hostetler, J. J. Pietron, R. W. Murray, T. G. Schaaff, J. T. Khoury, M. M. Alvarez, R. L. Whetten, *Science* **1998**, *280*, 2098–2101; e) A. S. K. Hashmi, G. J. Hutchings, *Angew. Chem.* **2006**, *118*, 8064–8105; *Angew. Chem. Int. Ed.* **2006**, *45*, 7896–7936; f) H. Häkkinen, *Nat. Chem.* **2012**, *4*, 443–455; g) Y. Pei, X. C. Zeng, *Nanoscale* **2012**, *4*, 4054–4072; h) H. Qian, M. Zhu, Z. Wu, R. Jin, *Acc. Chem. Res.* **2012**, *45*, 1470–1479; i) S. Knoppe, I. Dolamic, A. Dass, T. Burgi, *Angew. Chem.* **2012**, *124*, 7709–7711; *Angew. Chem. Int. Ed.* **2012**, *51*, 7589–7591.

[2] P. D. Jadzinsky, G. Calero, C. J. Ackerson, D. A. Bushnell, R. D. Kornberg, *Science* **2007**, *318*, 430–433.

[3] H. Häkkinen, M. Walter, H. Gronbeck, *J. Phys. Chem. B* **2006**, *110*, 9927–9931.

[4] a) M. W. Heaven, A. Dass, P. S. White, K. M. Holt, R. W. Murray, *J. Am. Chem. Soc.* **2008**, *130*, 3754–3755; b) M. Zhu, C. M. Aikens, F. J. Hollander, G. C. Schatz, R. Jin, *J. Am. Chem. Soc.* **2008**, *130*, 5883–5885.

[5] H. Qian, W. T. Eckenhoff, Y. Zhu, T. Pintauer, R. Jin, *J. Am. Chem. Soc.* **2010**, *132*, 8280–8281.

[6] C. Zeng, H. Qian, T. Li, G. Li, N. L. Rosi, B. Yoon, R. N. Barnett, R. L. Whetten, U. Landman, R. Jin, *Angew. Chem.* **2012**, *124*, 13291–13295; *Angew. Chem. Int. Ed.* **2012**, *51*, 13114–13118.

[7] R. C. Price, R. L. Whetten, *J. Am. Chem. Soc.* **2005**, *127*, 13750–13751.

[8] H. Qian, R. Jin, *Nano Lett.* **2009**, *9*, 4083–4087.

[9] Y. Zhang, S. Shuang, C. Dong, C. K. Lo, M. C. Paau, M. M. Choi, *Anal. Chem.* **2009**, *81*, 1676–1685.

[10] S. M. Reilly, T. Krick, A. Dass, *J. Phys. Chem. C* **2010**, *114*, 741–745.

[11] M. Zhu, H. Qian, R. Jin, *J. Am. Chem. Soc.* **2009**, *131*, 7220–7221.

[12] M. Zhu, H. Qian, R. Jin, *J. Phys. Chem. Lett.* **2010**, *1*, 1003–1007.

[13] H. Qian, Y. Zhu, R. Jin, *J. Am. Chem. Soc.* **2010**, *132*, 4583–4585.

[14] Z. Wu, M. A. MacDonald, J. Chen, P. Zhang, R. Jin, *J. Am. Chem. Soc.* **2011**, *133*, 9670–9673.

[15] A. Dass, *J. Am. Chem. Soc.* **2009**, *131*, 11666–11667.

[16] a) J. Akola, M. Walter, R. L. Whetten, H. Hakkinen, H. Gronbeck, *J. Am. Chem. Soc.* **2008**, *130*, 3756–3757; b) Y. Pei, Y. Gao, X. C. Zeng, *J. Am. Chem. Soc.* **2008**, *130*, 7830–7832; c) O. Lopez-Acevedo, H. Tsunoyama, T. Tsukuda, C. M. Aikens, *J. Am. Chem. Soc.* **2010**, *132*, 8210–8218.

[17] D. E. Jiang, M. Walter, J. Akola, *J. Phys. Chem. C* **2010**, *114*, 15883–15889.

[18] O. Lopez-Acevedo, J. Akola, R. L. Whetten, H. Gronbeck, H. Hakkinen, *J. Phys. Chem. C* **2009**, *113*, 5035–5038.

[19] D. E. Jiang, R. L. Whetten, W. D. Luo, S. Dai, *J. Phys. Chem. C* **2009**, *113*, 17291–17295.

[20] A. Tlahuice, I. L. Garzon, *Phys. Chem. Chem. Phys.* **2012**, *14*, 3737–3740.

[21] Y. Pei, Y. Gao, N. Shao, X. C. Zeng, *J. Am. Chem. Soc.* **2009**, *131*, 13619–13621.

[22] Y. Pei, R. Pal, C. Liu, Y. Gao, Z. Zhang, X. C. Zeng, *J. Am. Chem. Soc.* **2012**, *134*, 3015–3024.

[23] D. E. Jiang, *Chem. Eur. J.* **2011**, *17*, 12289–12293.

[24] M. Walter, J. Akola, O. Lopez-Acevedo, P. D. Jadzinsky, G. Calero, C. J. Ackerson, R. L. Whetten, H. Gronbeck, H. Hakkinen, *Proc. Natl. Acad. Sci. USA* **2008**, *105*, 9157–9162.

[25] a) W. Knight, K. Clemenger, W. A. de Heer, W. A. Saunders, M. Chou, M. L. Cohen, *Phys. Rev. Lett.* **1984**, *52*, 2141–2143; b) W. A. de Heer, *Rev. Mod. Phys.* **1993**, *65*, 611–676.

[26] K. Clemenger, *Phys. Rev. B* **1985**, *32*, 1359–1362.

[27] L. Cheng, J. Yang, *J. Chem. Phys.* **2013**, *138*, 141101.

[28] L. Cheng, C. Ren, X. Zhang, J. Yang, *Nanoscale* **2013**, *5*, 1475–1478.

[29] D. Y. Zubarev, A. I. Boldyrev, *Phys. Chem. Chem. Phys.* **2008**, *10*, 5207–5217.

[30] a) D. Y. Zubarev, A. I. Boldyrev, *J. Org. Chem.* **2008**, *73*, 9251–9258; b) A. P. Sergeeva, D. Y. Zubarev, H. J. Zhai, A. I. Boldyrev, L. S. Wang, *J. Am. Chem. Soc.* **2008**, *130*, 7244–7246; c) W. Huang, A. P. Sergeeva, H. J. Zhai, B. B. Averkiev, L. S. Wang, A. I. Boldyrev, *Nat. Chem.* **2010**, *2*, 202–206; d) L. J. Cheng, *J. Chem. Phys.* **2012**, *136*, 104301; e) Y. Yuan, L. Cheng, *J. Chem. Phys.* **2012**, *137*, 044308; f) D. Y. Zubarev, A. I. Boldyrev, *J. Phys. Chem. A* **2009**, *113*, 866–868.

[31] P. v. R. Schleyer, C. Maerker, A. Dransfeld, H. Jiao, N. J. R. van Eikema Hommes, *J. Am. Chem. Soc.* **1996**, *118*, 6317–6318.

[32] S. A. Malola, L. Lehtovaara, S. Knoppe, K. J. Hu, R. E. Palmer, T. Burgi, H. J. Hakkinen, *J. Am. Chem. Soc.* **2012**, *134*, 19560–19563.

[33] A. Das, T. Li, K. Nobusada, Q. Zeng, N. L. Rosi, R. Jin, *J. Am. Chem. Soc.* **2012**, *134*, 20286 – 20289.
[34] Gaussian 09 (Revision B.01), M. J. Frisch, et al. Gaussian, Inc., Wallingford, CT, **2009**.
[35] J. P. Perdew, K. Burke, M. Ernzerhof, *Phys. Rev. Lett.* **1996**, *77*, 3865 – 3868.
[36] U. Varetto, Molekel 5.4.0.8, Swiss National Supercomputing Centre, Manno, Switzerland, **2009**.

